Journal of Applied Polymer Science

Epoxy Resins Reinforced with TiO_2 Generated by Nonhydrolytic Sol-Gel Process

Davide Morselli,[1,2] Federica Bondioli,[1,3] Marco Sangermano,[1,4] Ignazio Roppolo,[1,5] Massimo Messori[1,2]

[1]Italian Interuniversity Consortium of Materials Science and Technology (INSTM), Via Giusti 9, 50121 Firenze, Italy
[2]Department of Engineering "Enzo Ferrari", University of Modena and Reggio Emilia, Via Vignolese 905/A, 41125 Modena, Italy
[3]Department of Industrial Engineering, University of Parma, Parco delle Scienze 181/A, 43124 Parma (I)
[4]Department of Applied Science and Technology, Polytechnic of Turin, Corso Duca degli Abruzzi 24, 10129 Torino, Italy
[5]Italian Institute of Technology, Center for Space and Human Robotics, Corso Trento 21, 10129, Torino, Italy
Correspondence to: M. Messori (E-mail: massimo.messori@unimore.it)

ABSTRACT: Innovative epoxy-titania nanocomposites were prepared starting from titania nanoparticles suspended in benzyl alcohol (BzOH) generated by nonhydrolytic sol–gel process from $TiCl_4$. The obtained suspensions were mixed with an epoxy resin (bisphenol A diglycidyl ether, DGEBA) and the formulations were cured in the presence of ytterbium(III) trifluoromethanesulfonate as cationic initiator. The thermally activated cationic ring-opening polymerization produced a three-dimensional network in which the suspending medium BzOH was covalently linked to the epoxy network according to the "activated monomer" mechanism during the propagation step. The presence of titania nanoparticles resulted in a reinforcing and stiffening effect due to both their hydrodynamic effect and, most important, a significantly higher cross-linking density of the composite material with respect to the unfilled epoxy resin. © 2014 Wiley Periodicals, Inc. J. Appl. Polym. Sci. **2014**, *131*, 40470.

KEYWORDS: crosslinking; nanoparticles; nanowires and nanocrystals; thermosets

Received 12 November 2013; accepted 18 January 2014
DOI: 10.1002/app.40470

INTRODUCTION

The field of organic–inorganic hybrid materials is of great interest thanks to the possibility to combine some peculiar mechanical and functional properties of both organic polymers and inorganic materials in a synergistic way by combining the different phases at a nanoscale. Organic–inorganic hybrid materials represent not only a new and exciting field of basic research but also offer perspectives for several new applications in different technological fields. The very large set of accessible hybrid materials span a wide spectrum of properties, which yield the emergence of innovative industrial applications in various domains such as optics, micro-electronics, transportation, health, energy, housing, and the environment among others.[1]

Concerning the specific area of thermoset or thermoplastic polymers reinforced/filled with metal oxide nanoparticles, it is well known that these nanoparticles, arising from flame pyrolysis or aqueous syntheses, cannot be easily dispersed in organic oligomers or polymers by using the conventional physical mixing processes, due to their hydrophilic character and strong tendency to agglomeration.

In this respect, organic–inorganic hybrid materials based on in situ generation of nanoparticles could represent an interesting alternative approach to design new composite materials. Among the different synthetic procedures,[2] the sol–gel chemistry represents one of the preferred ways for the preparation of organic–inorganic hybrids according to the so-called bottom-up approach. The sol–gel process is a chemical method used for the synthesis of inorganic metal oxides, initially employed to synthesize high purity inorganic networks as glasses and ceramic materials. This method can be applied at room temperature or slightly higher, becoming strategic when thermally degradable organic materials are involved in the process. The most used method is based on the so-called aqueous (or hydrolytic) sol–gel process, which is generally based on metal alkoxides as precursors and can be schematically divided into two steps: the first one named hydrolysis, which produces hydroxyl groups, and the second one named condensation, that involves the polycondensation of hydroxyl groups and residual alkoxyl groups to form a three-dimensional network.[3] The presence in the reactive system of an organic oligomer or polymer (having or not suitable groups reactive towards to the sol–gel process) leads to the

formation of organic–inorganic hybrid structures in which the inorganic oxide and the organic phases are intimately mixed each other.

Alternatively to the aqueous route, the so-called nonhydrolytic sol–gel (NHSG) reaction can be used to obtain very pure and crystalline metal oxides.[4] As well as the aqueous route, the NHSG process is divided in two steps. The first step involves the reaction of a metal halide or a metal alkoxide with an organic oxygen donor (such as alcohols, ether, etc.) The second step (condensation) can follow different pathways depending on the employed oxygen donor. In principle, the NHSG route offers access to a wide range of organic–inorganic hybrid materials similar to those accessible using the hydrolytic route. In practice, differences arising from the nature of the precursors, possible solvent choice, and the different mechanisms of the reactions may dictate the type of hybrid, which can be prepared by either route. With respect the hydrolytic counterpart, it is recognized that NHSG process is potentially solvent-free, without problems with hydrophobic substances and particularly suitable for water-sensitive species. On the other hand, the formation of alkyl halide and/or alkyl ethers as by-products and the potential incompatibility with oxygen-containing species have to be taken into account as possible negative aspects.[5]

The preparation of polymer-matrix nanocomposites exploiting the NHSG process for the generation of metal oxide nanoparticles was recently proposed in the literature as described in the follows.

The preparation of poly(methyl methacrylate) (PMMA)/titania composites was recently suggested by Messori et al. exploiting the reaction of $TiCl_4$ and benzyl alcohol or tert-butanol in the presence of preformed PMMA.[6,7] The synthesis of PMMA/silica composites were also proposed with a very similar approach through the reaction between $SiCl_4$ and ethanol.[8] In comparison with the samples prepared by traditional sol–gel route, these hybrids exhibit higher optical transparency and better thermal stability.

Transparent PMMA nanocomposites containing silica and titania with enhanced thermal stability were also prepared starting from methyl methacrylate and 3-(trimethoxysilyl)propyl methacrylate as polymethacrylate monomers and tetraethoxysilane and titanium ethoxide as inorganic oxides precursors.[9] A similar synthetic approach was also proposed by Du et al. for the preparation of PMMA/silica/titania and PMMA/silica/zirconia ternary nanocomposites with improved thermal and thermo-oxidative stabilities for potential applications in optical devices.[10–12]

Polypropylene/silica,[13] polyphenylsulfone/silica,[14] polyimide/titania,[15] and polyimide/silica/titania[16] are other examples of thermoplastic-matrix nanocomposites in which the filler nanoparticles were obtained through NHSG process.

Concerning thermoset organic matrices, silica-based organic–inorganic hybrid resins were synthesized by NHSG from 3-glycidoxypropyltrimethoxysilane and diphenylsilanediol (DPSD) at a fixed amount of (20 mol %) phenyltrimethoxysilane using barium hydroxide as a catalyst for potential use in encapsulating commercial phosphor powder for white LEDs.[17] Also cycloaliphatic epoxy oligosiloxane resins were proposed as UV-curable resins for application in encapsulation of organic light emitting devices.[18]

The NHSG condensation reaction of methacryloxypropyl trimethoxysilane and DPSD was exploited in order to synthesize nano-structured molecular units for the preparation of hybrid organic/inorganic coatings in the presence of suitable thermal and photo-initiators.[19]

In a recent work, we reported an innovative procedure based on the preparation of titania nanoparticles suspended in benzyl alcohol and the mixing of this suspension with UV-curable cycloaliphatic epoxy resin.[20] The cationic photo-polymerization produced a three-dimensional network in which the suspending medium benzyl alcohol was covalently linked to the epoxy network according to the "activated monomer" mechanism[21] during the propagation step in the cationic ring-opening polymerization. The presence of titania resulted in a reinforcing and stiffening effect due to both the presence of inorganic nanofillers and, most importantly, a higher cross-linking density of the composite material with respect to the pristine epoxy matrix.

Other than mechanical enhancements, titania-polymer hybrids have also found application in many different fields such as antibacterial materials,[22,23] UV filters,[24] tunable reflective index materials,[25] and in the field of hybrid organic solar cells.[26] Furthermore, as suggested by Zhao et al.,[27] in his review, polymer/TiO_2 composites play an important key role also in environmental applications field.

In this work, the same approach was used in order to verify the possibility to incorporate titania suspensions in benzyl alcohol and epoxy resin by means of a thermally activated cationic polymerization instead of the UV-curing process.

EXPERIMENTAL

Materials

Bisphenol A diglycidyl ether (DGEBA, Dow D.E.R.™ 332 with an epoxide equivalent weight of 172–176), titanium(IV) chloride ($TiCl_4$), benzyl alcohol (BzOH), propylene carbonate (PC), ytterbium(III) trifluoromethanesulfonate hydrate ($Yb(OTf)_3$), ethanol, chloroform, acetone, and diethyl ether were purchased by Sigma Aldrich (Milan, Italy). All materials were high purity reactants and were used as received without any further purification.

Preparation of Titania Suspensions

According to a previously reported[20] synthetic procedure, a given quantity of $TiCl_4$ (see composition details in Table I) was added drop-wise to 1.50 g of BzOH at room temperature under vigorous stirring. The reaction was left stirring at room temperature for 15 min and then heated to 70°C for 24 h. After reaction a stable suspension was obtained. Part of the obtained suspensions was centrifuged at 4000 rpm for 15 min. The so-obtained powders were carefully washed twice using chloroform, twice by acetone and once by diethyl ether, sonicating for 10 min every time that fresh solvent was added. Finally they were

Table I. Composition of the Prepared Suspensions

TiO_2 suspension code	$TiCl_4$ (g)	BzOH (g)	BzOH/$TiCl_4$ molar ratio	Nominal TiO_2 (g)
S15	0.36	1.50	7.3	0.15
S25	0.59		4.5	0.25
S50	1.19		2.2	0.50

dried at 80°C for 8 h under dynamic vacuum in order to obtain titania powders for characterizations.

Preparation of Epoxy-Titania Composites

A typical thermally curable formulation was prepared by mixing titania suspension, epoxy resin, and a solution of $Yb(OTf)_3$ in PC (1:3 wt/wt ratio) as thermal cationic initiator (see composition details in Table II) by using a T18 Ultra-Turrax® Ika disperser (5 min mixing time) followed by 15 min treatment in an ultrasonic bath. The formulations were cast into silicone molds having cavities with dimension 4 × 1 × 0.2 cm^3. All the formulations were cured at 120°C for 25 min and a post-curing 20 min long at 160°C was subsequently applied.

Characterization of Titania Powders

The synthesized titania powders were analyzed with a computer-assisted conventional Bragg-Brentano diffractometer using the Ni-filtered CuKα monochromatic radiation ($\lambda = 1.5418$ Å) (PANalytical, X'Pert PRO difractometre) to identify the crystalline phase. The X-ray diffraction (XRD) patterns were collected at room temperature in a 2θ range of 10–90°, with a scanning rate of 0.005° s^{-1} and a step size of 0.02°. Crystallite size was estimated from X-ray line broadening measurements; using the TiO_2 (1,0,1) diffraction line according to the Sherrer formula[28]:

$$D = \frac{0.9 \cdot \lambda}{\beta \cdot \cos\theta} \quad (1)$$

where D is the crystallites size, λ is the wavelength of the X-ray (Cu Kα, 1.542 Å), θ is the diffraction angle, and β is the half width.

Particles morphology was examined by transmission electron microscopy, TEM (Jeol, JEM 2010). One drop of the obtained suspensions was diluted in 1 mL of ethanol, sonicated for 15 min, and placed on a copper grid covered with a transparent polymer, followed by drying. TEM images were analyzed and processed by ImageJ open-source software in order to obtain an average particles size.

The amount of organic volatile fractions on the particles surface was evaluated by thermo-gravimetric analysis measuring the percentages of weight loss after a treatment at high temperature in an electric furnace (Optolab – FS5). The treatment was carried out at 600°C for 2 h, up to constant mass was reached.

To qualitatively investigate the residual organic groups and/or free –OH chemically bonded on the particles surfaces an FTIR analysis was performed on the obtained powders. The analysis was carried out using an FTIR VERTEX 70 spectrometer (Bruker) in ATR mode from 4000 to 500 cm^{-1}, equipped with a diamond crystal.

The specific surface area (SSA) and density (ρ) of the powders were determined by the BET method[29] (Gemini 2360 apparatus, Micromeritics, Norcross) and by Helium pycnometer (Accupic 1330 apparatus, Micromeritics, Norcross), respectively. Assuming the particles were closed spheres, the average particle size was also calculated from the data of specific surface area, using the eq. (2):[30]

$$\phi = \frac{6}{\mathrm{SSA} \cdot \rho} \quad (2)$$

where ϕ is the average diameter of the spherical particle, SSA is the surface area of the powder, and ρ is the experimental density of powders.

Characterization of Epoxy-Titania Composites

The actual titania contents were evaluated by thermo-gravimetric analysis, calculating the amount of residual titania after a treatment at high temperature in an electric furnace (Optolab – FS5). The treatment was carried out at 600°C for 4 h, up to constant mass was reached.

The prepared samples were broken in liquid nitrogen and the cross-sections were analyzed by field emission scanning electron microscopy (FESEM, FEI STRATA DB235M Dual beam FIB-SEM instrument) by the application of an accelerating voltage of 15 kV. The cross sections were previously coated with gold (thickness 15 nm) by an electro-deposition method to impart electrical conduction. The obtained images were analyzed and processed by ImageJ open-source software.

Gel content was determined on the cured specimens by measuring the weight loss after 24 h extraction with chloroform at room temperature, according to an adaptation of the ASTM D2765-84 technical standard.

Dynamic-mechanical thermal analyses (DMTA) were carried out on an MK III Rheometrics Scientific Instrument at 1 Hz

Table II. Composition of the Thermally Curable Composite Formulations

Composite code	DGEBA (g)	$Yb(OTf)_3$/PC (g)	TiO_2 suspension	Nominal TiO_2 (phr)	Actual TiO_2 (phr)[a]	Actual TiO_2 (wt %)[a]
DGEBA-T0	5.0	0.15	only BzOH (1.50 g)	–	–	–
DGEBA-T3			S15	3	2.8	2.7
DGEBA-T5			S25	5	4.1	3.9
DGEBA-T10			S50	10	8.0	7.4

[a] Actual titania content experimentally determined by thermogravimetric analysis.

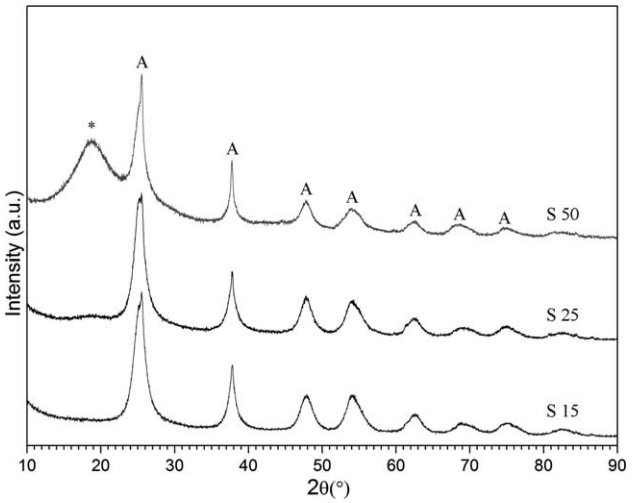

Figure 1. XRD patterns of titania powders obtained after drying and washing of the corresponding suspensions (A: anatase; * Unknown peak).

frequency in the tensile configuration employing a heating rate of 10°C min^{-1}. The storage modulus, E', and the loss factor, tanδ, were measured from 0°C up to the temperature at which the rubbery state was attained. The glass transition temperature ($T_{g,DMTA}$) was assumed as the maximum of the loss factor curve.

Differential scanning calorimetry (DSC) was carried out by a Thermal Analysis TA2010 Instruments at a scanning rate of 5°C min^{-1} from 0°C to 200°C under nitrogen flow.

The filler volume fractions of the cured nanocomposites were calculated taking into account the experimentally determined density values of pristine epoxy "DGEBA-T0" (1.189 g cm^{-3}) and titania particles under the assumption of density additivity.

RESULTS AND DISCUSSION

Characterization of Titania Powders

XRD analysis (Figure 1) showed that titania powders obtained after drying and washing of the corresponding suspensions are characterized by the presence of a crystalline phase (anatase JCPDS file 01–075-1537). The patterns showed, moreover, the presence of an unknown phase, attributable to the organic chains on the particles' surface, whose content decreases by increasing the initial BzOH/$TiCl_4$ molar ratio.

The average crystal size of the synthesized titania powders, calculated by the Sherrer's formula (Table III), was around 10 nm with a not meaningful increase as the BzOH/$TiCl_4$ molar ratio is decreased.

The shape and the dimensions of the primary particles were also evaluated by TEM. Typical TEM micrographs, already reported in a previous paper,[20] showed that the synthesized powder has nano-structured rather regular shape. The evaluated average particle size, by analyzing images, is 10 ± 4 nm in good agreement with data calculated by Scherrer's equation.

Taking into account that the adopted washing step for obtaining the titania powders should ensure the complete elimination of unlinked organic substances, the presence of an organic fraction chemically linked and/or strongly adsorbed to the titania particles was investigated by measuring the weight loss after heating at 600°C. The inorganic residue values reported in Table III show that the powders obtained from S15 and S25 suspensions were comprised of about 70 wt % of inorganic (titania) phase while the powder obtained from S50 suspension contained a significantly higher organic content (about 76 wt %).

The presence of an organic phase was also confirmed by FTIR analysis (Figure 2), which showed the typical signals attributable to uncondensed benzyl groups remained on particles surface. All spectra in Figure 2 showed a large band centered around 3200 cm^{-1} due to the stretching vibration of the –OH on the particles surface and related bending at 1600 cm^{-1}, whereas below 900 cm^{-1} the typical broad band due to Ti—O—Ti vibrations was observed.[31] Moreover, in Figure 2 is clearly shown that the powders are functionalized by benzyl groups presenting the C—H aromatic stretching between 3100 and 3000 cm^{-1}, C—H aliphatic stretching 2950–2800 cm^{-1} and the related bending vibration in the range 1500–1400 cm^{-1} that match perfectly with the benzyl alcohol spectrum. As expected, intensity of these signals, above described, increase when the BzOH/$TiCl_4$ ratio decreases consolidating the XRD and thermo-gravimetric results.

Aforementioned the experimental density (ρ_{exp}) values of the powders determined by pycnometer are relatively low, ranging from 2.60 to 1.39 g cm^{-3}, but on the basis of these evidences, they can be considered as deriving from hybrid materials comprised of titania and organic substances presumably covering the surface of the inorganic particles. In order to determine the actual density of the titania particles without the contribution of the organic component, density values were corrected by assuming BzOH as main component of the organic phase (with a density $\rho_{BzOH} = 1.045$ g cm^{-3}) and the density additivity rule, according to the following equation:

Table III. Properties of Titania Powders Obtained from the Corresponding Suspension: Mean Crystallite Size as Determined by XRD Pattern Elaboration, Specific Surface Area (SSA), Residue After Organic Phase Combustion and Experimental and Corrected Densities (ρ_{exp}, ρ_{TiO2}) Corrected on the Basis of the Actual Inorganic Content

TiO_2 suspension code	Average crystal size from XRD (nm)	SSA (m^2 g^{-1})	Residue at 600°C (wt %)	ρ_{exp} (g cm^{-3})	ρ_{TiO2} (g cm^{-3})
S15	9	118	70.4	2.60	3.25
S25	10	48	69.6	2.01	2.44
S50	11	26	24.1	1.39	2.49

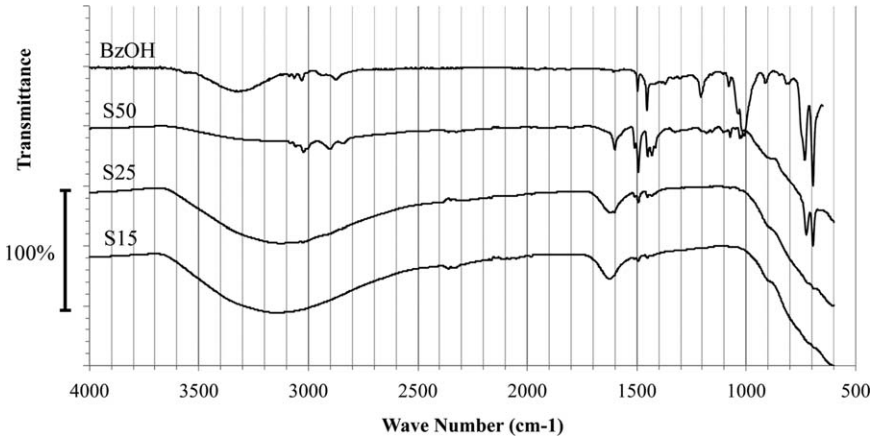

Figure 2. FTIR spectra of the synthesized powders and BzOH as comparison.

$$\rho_{exp} = \rho_{TiO2} \cdot W_{TiO2} + \rho_{BzOH} \cdot W_{BzOH} \quad (3)$$

in which w_{TiO2} and w_{BzOH} are the weight fraction of titania and BzOH, respectively. These corrected values (Table III) were used for the calculation of the volume composition of the prepared epoxy-titania nanocomposites.

Specific surface area SSA values range from a maximum of 118 $m^2\ g^{-1}$ for titania obtained from S15 suspension to a minimum of 26 $m^2\ g^{-1}$ for titania powders obtained from S50 suspension. This could be caused by the residual organic substances that create a real capping structure on the particles surface, which is able to decrease SSA making less available the surface. That is consistent with results found by XRD, FTIR, and TG that showed an increase of this organic layer when the BzOH/$TiCl_4$ ratio decreases. Furthermore, average diameters of titania powders were calculated from SSA and density values (eq. (2)) and, accordingly, the average powders diameter increases from a minimum of 19 nm to a maximum of 167 nm. The differences between the average particle size as determined by X-ray line broadening and as elaborated by SSA and density values is a strong evidence of grains agglomeration. Of course this conclusion is to be applied to the dried powders and does not imply that in the starting fluid suspensions the nanoparticles were likewise aggregated.

Characterization of Epoxy-Titania Composites

Thermo-gravimetric analyses showed actual titania contents (Table II) are rather closed to the nominal ones proving that the employed procedure is an effective alternative to produce composites avoiding the conventional mixing methods.

Gel content was determined in order to evaluate the effect of the presence of the titania suspension on the cross-linked structure (Table IV).

Gel content values were extremely high (equal or higher than 99.0%) for all investigated samples suggesting the formation of a fully developed three-dimensional network (with a negligible amount of extractable sol fraction) even in the case of a relatively high BzOH content. This important result suggested that both "active chain end" and "activated monomer" mechanisms (see Scheme 1) occurred during the propagation step in the cationic ring-opening polymerization leading to a quantitative incorporation of BzOH (and corresponding by-products of NHSG reaction) within epoxy network, as indicated by the absence of species extractable in chloroform.

FESEM characterization of the composites permitted to evaluate the distribution and aggregation of titania particles in the matrix. Typical FESEM micrographs of epoxy-titania composites fracture surface having titania content of 2.8 and 8.0 phr, respectively, are reported in Figure 3. The fracture surfaces (characteristic also for the other compositions) showed the presence of a homogeneous dispersed phase attributable to a titania rich phase as indicated by EDX analysis (here not reported). Even though the filler is well distributed, FESEM images also showed some particles agglomeration in small titania domains. The sample DGEBA-3T [Figure 3(a)] showed that

Table IV. Properties of the Thermally Cured Composites: Gel Content (G), Glass Transition Temperature from DSC ($T_{g,DSC}$), Glass Transition Temperature from DMTA ($T_{g,DMTA}$), Damping (Expressed as Maximum Value of tanδ, tanδ_{max}), Storage Moduli Measured at $T = 40°C$ and $T = T_g + 40°C$ ($E'_{T=40°C}$, and $E'_{T=Tg+40°C}$), Network Density (Average Molecular Weight Between Two Adjacent Cross-Linking Points, M_C), and Effective Thickness of the Particle–Matrix Interfacial Region (ΔR)

Composite code	G (wt %)	$T_{g,DSC}$ (°C)	$T_{g,DMTA}$ (°C)	tanδ_{max}	$E'_{T=40°C}$ (GPa)	$E'_{T=Tg+40°C}$ (MPa)	M_C (g/mol)	ΔR (nm)
DGEBA-T0	99.0	50	75	1.721	0.458	0.926	12,800	-
DGEBA-T3	99.7	67	100	1.436	0.546	2.530	5,000	8
DGEBA-T5	99.7	73	113	1.030	0.713	5.014	2,600	14
DGEBA-T10	98.8	86	139	0.758	0.549	7.071	2,000	12

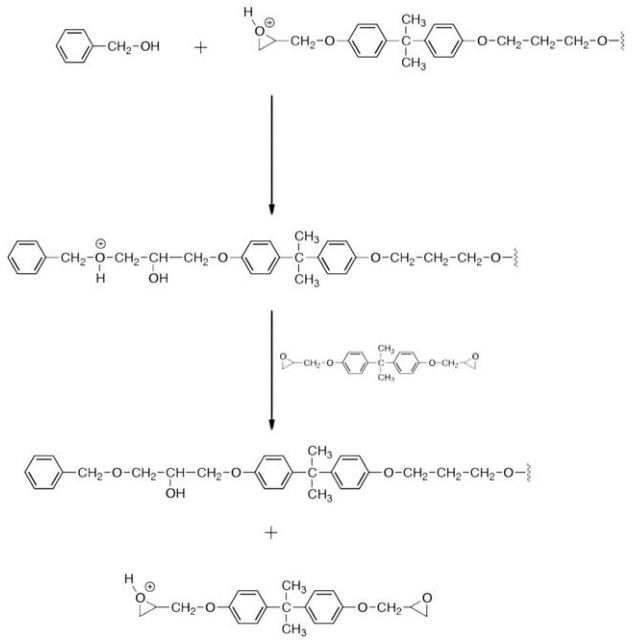

Scheme 1. Schematic of the "activated monomer" mechanism.

the average size of these aggregates is 405 ± 101 nm, whereas bigger agglomerates, ranging from 470 nm to 1.1 μm, were detected in the case of DGEBA-10T [Figure 3(b)]. This phenomenon was probably due to the common strong tendency of titania particles to aggregate that was also reported in a previous article.[20] Anyway it can be considered a good results, taking into account that homogeneous filler distributions was reached for all samples, avoiding the use of any coupling agent and/or long and complicated dispersion treatments, for samples production.

Glass transition temperature (T_g), damping (expressed as maximum value of loss factor, $\tan\delta_{max}$) and storage modulus (E') values of thermally cured composites obtained by DMTA are reported in Table IV.

The obtained results showed that the dynamic-mechanical properties of composites were significantly affected by the titania content. As expected in the case of polymers filled with particles, the incorporation of rigid fillers into a polymeric matrix made difficult the movement of the polymer chains leading to a damping decrement and a shift of T_g values to higher temperatures. In the present work, as already reported in Ref. 20, a significant reduction of damping (quantified as $\tan\delta_{max}$) was observed by increasing the titania concentration in the composites, together with a very significant increment in T_g values. The glass transition temperature of unfilled epoxy (75°C) increased up to 100, 113, and 139°C for DGEBA-T3, DGEBA-T5, and DGEBA-T10, respectively. Such increases in T_g can be attributed to the constrained chain mobility by well-dispersed filler.

The general increase in T_g and decrease in loss factor $\tan\delta_{max}$ by increasing the titania content can be also considered as an indirect evidence of the presence of a strong filler-matrix interface. Kim et al.[32] reported the preparation and the characterization of epoxy-based composites containing inorganic nanoparticles functionalized or not functionalized with suitable coupling agents and reported that composites with weak filler-matrix interface exhibit essentially no modification in T_g and damping with filler contents, opposite to composites with strong filler-matrix interface which show a systematic increase of T_g and decrease of loss factor with filler content.

The storage moduli E' measured in the glassy state (that is at a temperature of 40°C) were slightly influenced by the presence and the amount of titania. $E'_{T=40°C}$ values for composites were always higher than that of unfilled DGEBA-T0 (0.458 GPa) with the maximum value of 0.713 GPa for composite with intermediate filler content (DGEBA-T5). A much stronger influence due to the presence of titania was observed in the rubbery state. In this respect, it is very interesting to note that the storage moduli E' measured above the glass transition temperature (that is at a temperature of $T_g + 40$°C) increased significantly by increasing the titania content. $E'_{T=Tg+40°C}$ values of DGEBA-T0

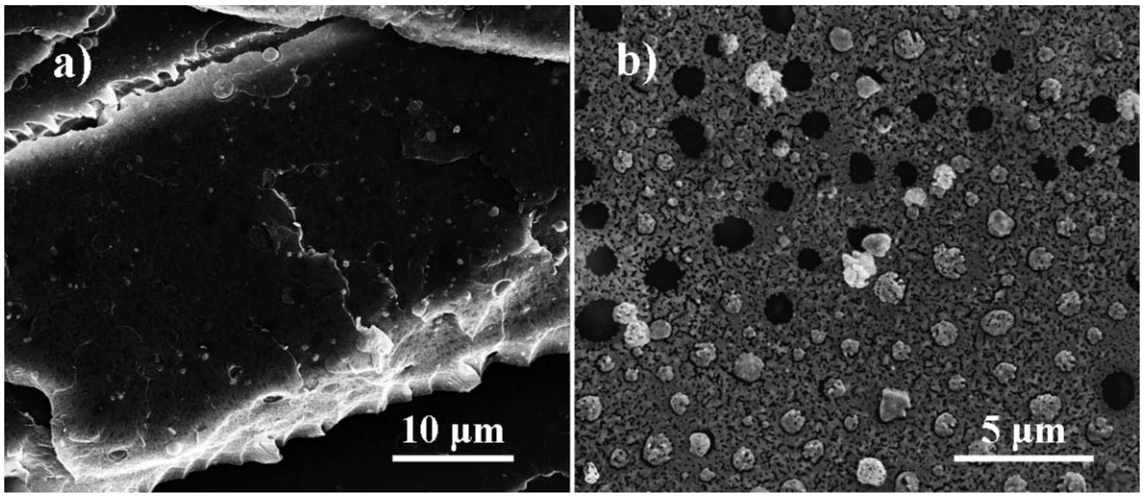

Figure 3. FESEM micrograph of the fractured surface of DGEBA-3T (a) and DGEBA-10T (b).

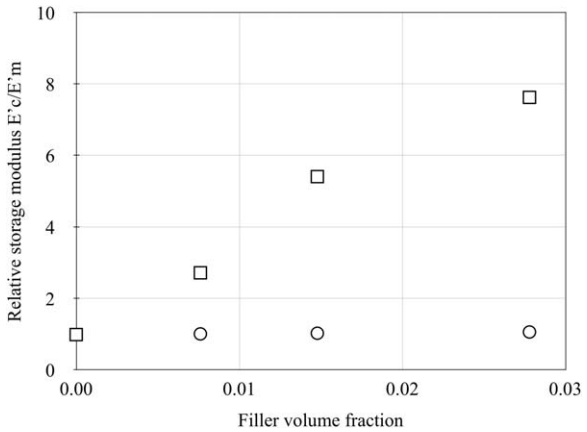

Figure 4. Relative storage modulus dependence on the titania particles content (v/v): (□) experimental values and (○) prediction by generalized Kerner equation.

(0.926 MPa) raised up to 2.530, 5.014, and 7.071 MPa for DGEBA-T3, DGEBA-T5, and DGEBA-T10, respectively.

The reduced storage modulus (that the ratio between the moduli of the composite and of the matrix, respectively) measured in the rubbery region as a function of titania volume fraction is reported in Figure 4. To compare the experimental results with data predicted with well known models for composites materials, the generalized Kerner equation for the reduced modulus of filled polymers was applied in order to evaluate its dependence on the nanoparticles content:

$$\frac{E'}{E'_1} = \frac{1 + A \cdot B \cdot \phi_2}{1 - B \cdot \Psi \cdot \phi_2} \tag{4}$$

in which E' and E'_1 are the storage moduli of composite and unfilled epoxy, respectively.

The constant A, in the case of spherical filler particles and for any Poisson's ratio v of the matrix, is defined as:

$$A = \frac{7 - 5v}{8 - 10v} \tag{5}$$

The constant B depends on the ratio between filler and matrix moduli and it can be approximated to 1 for very large moduli ratios. The parameter Ψ is a reduced concentration term which depends on the maximum packing fraction of the particles (ϕ_m) according to the following definition:

$$\Psi = 1 + \frac{1 - \phi_m}{\phi_m^2} \cdot \phi_2 \tag{6}$$

in which ϕ_2 is the filler volume fraction.

In this study, the Poisson's ratio v of the matrix and the maximum packing fraction of the particles ϕ_m were taken equal to 0.5 (epoxy in the rubbery state) and to 0.601 (random loose packing, non agglomerated packing configuration), respectively.[33]

Data indicated a very important increment of reduced storage modulus with respect to the values predicted by the generalized Kerner equation. Taking into account that, in the rubbery region temperature range, the modulus values are mainly governed by the cross-linking density of the network, a considerable increase of this last parameter has to be considered in the presence of *in situ* generated titania. In other words, titania nanoparticles generated by NHSG process acted not only as rigid reinforcing filler but also as cross-linking points, increasing the cross-linking density of the composite material with respect to the pristine epoxy matrix.

To further investigate this aspect, the network densities (that is the average molecular weight between two adjacent cross-linking points, M_C) were determined in the rubbery region from the storage modulus values at $T_g + 40°C$ by using the following relationship:

$$E'_{Tg+40°c} = 3 \cdot q \cdot n \cdot RT = 3 \cdot q \cdot \left(\frac{\rho}{M_c}\right) \cdot RT \tag{7}$$

where, q is the front factor (usually equal to 1), n is the apparent cross-linking density, R is the gas constant ($R = 8.314$ J K^{-1} mol^{-1}), ρ is the density of the material, and T is the absolute temperature in K.[34] Originally, eq. (7) was used for single-phase materials, but it also gives very good results for biphasic systems.[34,35] However, the values obtained by this formula should be intended only for comparing the network density of the samples investigated in this work.

The calculated values of polymer molecular weight between two cross-linking points, M_C, are reported in Table IV. The network density increases and M_C decreases as the titania content increases. According to the dynamic–mechanic behavior already discussed, the presence of the rigid filler increases the local concentration of the cross-linking points and increases the network density in the composite compared to the neat matrix. As already mentioned, this behavior could be tentatively explained taking into account that the in situ generation of titania and subsequent polymerization of the suspending medium resulted in a very strong filler–matrix interaction with a significant improvement of the cross-linking density due to the titania contribution which in turn incremented the glass transition temperature and the modulus values in the rubbery region.

Thermal properties trend, of the thermally cured materials by DSC analysis, (see Table IV) is in good agreement with the obtained data by DMTA analysis, showing $T_{g,DSC}$ values of unfilled epoxy DGEBA-T0 (50°C) increasing up to 67, 73, and 86°C for DGEBA-T3, DGEBA-T5, and DGEBA-T10, respectively.

From the reduced damping values, the thickness of the polymer layer immobilized onto the titania nanoparticles surface was estimated at a temperature below glass transition temperature (35°C) by using the following equations:

$$\frac{\tan\delta}{\tan\delta_1} = 1 - P \cdot \phi_2 \tag{8}$$

$$P = \left(1 + \frac{\Delta R}{R}\right)^3 \tag{9}$$

in which $\tan\delta$ and $\tan\delta_1$ are the loss factors referred to the composite and to the pristine matrix, respectively, ϕ_2 is the filler volume fraction, R is the radius of the dispersed particles, and P is a correction parameter related to the effective thickness of the particle-matrix interfacial region ΔR.[36] Even if overestimated due to the presence of not negligible amount of organic

component, the average diameters of titania crystallites reported in Table III were used for the calculation. The calculated values of the layer thickness ΔR for all the samples are shown in Table IV. A relative thick layer was calculated for the composites (values of ΔR ranging from 8 to 14 nm that is of the same order of particles' diameter). The values here calculated are of the same order of magnitude of data reported by Friedrich et al. for epoxy/alumina nanocomposites prepared by mechanical dispersion of preformed alumina nanoparticles treated with different silane coupling agents.[34] Authors reported values of thickness of the particle-matrix interfacial region in the range 40–60 nm for alumina nanoparticles having diameter of 40 nm.

The relatively high values of the effective thickness (referred to the particles' diameter) of the titania-epoxy interfacial region here reported seem to be in good agreement with the already discussed strong filler-matrix interaction responsible of the significant improvement of the cross-linking density.

Interestingly, ΔR values here reported are generally higher than those determined for composites with similar titania particles but different epoxy resin (3,4-epoxycyclohexylmethyl-3,4-epoxycyclohexanecarboxylate, CE) and curing condition (UV curing),[20] indicating a higher stiffening at the particle-matrix interface due to the aromatic character of epoxy precursor (DGEBA instead of CE) and/or the curing method (thermal curing instead of radiation curing).

CONCLUSIONS

Suspensions of titania nanoparticles in benzyl alcohol were synthesized by means of nonhydrolytic sol–gel (NHSG) process, mixed with an epoxy resin (DGEBA), and subsequently cured through a thermally activated cationic polymerization. Gel content analysis demonstrated that all organic species (benzyl alcohol and corresponding by-products) were covalently linked to the epoxy network, suggesting that also the "activated monomer" mechanism was active during the propagation step in the cationic ring-opening polymerization.

The presence of titania increased significantly both glass transition temperature and modulus (in the rubbery region) and decreased the damping (expressed as the maximum value of tanδ). The dynamic–mechanical analysis and the nanoindentation analysis showed a significant increment of the mechanical properties which could be attributed to both the presence of a rigid filler with higher mechanical properties with respect to the epoxy matrix (hydrodynamic effect) and an increment of cross-linking density due to the titania nanoparticles generated by NHSG process which act as a cross-linking densifier.

ACKNOWLEDGMENTS

Ms. Elisa Parmeggiani is gratefully acknowledged for her support to experimental work.

REFERENCES

1. Sanchez, C.; Belleville, P.; Popall, M.; Nicole, L. *Chem. Soc. Rev.* **2011**, *40*, 696.
2. Sanchez, C.; Julian, B.; Belleville, P.; Popall, M. *J. Mater. Chem.* **2005**, *15*, 3559.
3. Brinker, C. J.; Shrerer, G. W. Sol-Gel Science: The Physics and Chemistry of Sol-Gel Processing; Academic Press: New York, **1990**.
4. Bilecka, I.; Niederberger, M. *Electrochimica Acta* **2010**, *55*, 7717.
5. Hay, J. N.; Raval, H. M. *Chem. Mater.* **2001**, *13*, 3396.
6. Morselli, D.; Bondioli, F.; Fiorini, M.; Messori, M. *J. Mater. Sci.* **2012**, *47*, 7003.
7. Morselli, D.; Messori, M.; Bondioli, F. *J. Mater. Sci.* **2011**, *46*, 6609.
8. Song, X.; Wang, X.; Wang, H.; Zhong, W.; Du, Q. *Mater. Chem. Phys.* **2008**, *109*, 143.
9. Kuan, H.-C.; Chiu, S.-L.; Chen, C.-H.; Kuan, C.-F.; Chiang, C.-L. *J. Appl. Polym. Sci.* **2009**, *113*, 1959.
10. Wang, H.; Meng, S.; Xu, P.; Zhong, W.; Du, Q. *Polym. Eng. Sci.* **2007**, *47*, 302.
11. Wang, H.; Xu, P.; Meng, S.; Zhong, W.; Du, W.; Du, Q. *Polym. Degrad. Stabil.* **2006**, *91*, 1455.
12. Wang, H.; Xu, P.; Zhong, W.; Shen, L.; Du, Q. *Polym. Degrad. Stabil.* **2005**, *87*, 319.
13. Qian, J.; Zhang, H.; Cheng, G.; Huang, Z.; Dang, S.; Xu, Y. *J. Sol-Gel Sci. Technol.* **2010**, *56*, 300.
14. Licoccia, S.; Di, V. M. L.; D'Epifanio, A.; Ahmed, Z.; Bellitto, S.; Marani, D.; Mecheri, B.; de, B. C.; Trombetta, M.; Traversa, E. *J. Power Sources* **2007**, *167*, 79.
15. Saeed, M. A.; Lodhi, Z. H.; Khan, A.-U.; Asghar, W. *Adv. Mater. Res. (Durnten-Zurich, Switz.)* **2011**, *326*, 88.
16. Wang, H.; Zhong, W.; Xu, P.; Du, Q. *Compos. Part A* **2005**, *36*, 909.
17. Jana, S.; Lim, M. A.; Baek, I. C.; Kim, C. H.; Seok, S. I. *Mater. Chem. Phys.* **2008**, *112*, 1008.
18. Jung, K.; Bae, J.-Y.; Park, S. J.; Yoo, S.; Bae, B.-S. *J. Mater. Chem.* **2011**, *21*, 1977.
19. Dire, S.; Tagliazucca, V.; Brusatin, G.; Bottazzo, J.; Fortunati, I.; Signorini, R.; Dainese, T.; Andraud, C.; Trombetta, M.; Di, V. M. L.; Licoccia, S. *J. Sol-Gel Sci. Technol.* **2008**, *48*, 217.
20. Morselli, D.; Bondioli, F.; Sangermano, M.; Messori, M. *Polymer* **2012**, *53*, 283.
21. Kubisa, P. *J. Polym. Sci. Part A: Polym. Chem.* **2003**, *41*, 457.
22. Shah, M.S.A.S.; Nag, M.; Kalagara, T.; Singh, S.; Manorama, S. V. *Chem. Mater.* **2008**, *20*, 2455.
23. Kubacka, A.; Serrano, C.; Ferrer, M.; Lünsdorf, H.; Bielecki, P.; Cerrada, M. L.; Fernández-García, M.; Fernández-García, M. *Nano Lett.* **2007**, *7*, 2529.
24. Nussbaumer, R.J.; Caseri, W.R.; Smith, P.; Tervoort, T. *Macromol. Mater. Eng.* **2003**, *288*, 44.
25. Antonello, A.; Brusatin, G.; Guglielmi, M.; Bello, V.; Mattei, G.; Zacco, G.; Martucci, A. *J. Nanopart. Res.* **2011**, *13*, 1697.
26. Bouclé, J.; Ravirajan, P.; Nelson, J. *J. Mater. Chem.* **2007**, *17*, 3141.

27. Zhao, X.; Lv, L.; Pan, B.; Zhang, W.; Zhang, S.; Zhang, Q. *Chem. Eng. J.* **2011**, *170*, 381.

28. Klug, P.; Alexander, L. E. X-Ray Diffraction Procedure; Wiley: New York, **1954**.

29. Brunauer, S.; Emmett, P. H.; Teller, E. *J. Am. Chem. Soc.* **1938**, *60*, 309.

30. Kodera, K. In: Powders (Theory and Applications); Kubo, K., Suito, E., Nakagawa, Y., Hayakawa, S., Eds.; Maruzen: Tokyo, **1962**.

31. Velasco, M. J.; Rubio, F.; Rubio, J.; Oteo, J. L. *Thermochim Acta* **1999**, *326*, 91.

32. Kang, S.; Hong, S. I.; Choe, C. R.; Park, M.; Rim, S.; Kim, J. *Polymer* **2001**, *42*, 879.

33. Nielsen, L. E.; Landel, R. F. Mechanical Properties of Polymers and Composites, 2nd ed.; Marcel Dekker: New York, **1994**.

34. Vassileva, E.; Friedrich, K. *J. Appl. Polym. Sci.* **2003**, *89*, 3774.

35. Levita, G.; Depetris, S.; Marchetti, A.; Lazzeri, A. *J. Mater. Sci.* **1991**, *26*, 2348.

36. Iisaka, K.; Shibayama, K. *J. Appl. Polym. Sci.* **1978**, *22*, 3135.